Supporting information

Design of phase change materials with carbon aerogel composite for multi-responsive thermal energy capture and storage

Keyan Sun,[a,d] Yan Kou,[a] Hongsheng Dong,[a] Sheng Ye,[b] Donghui Zhao,[e] Jian Liu,*[b,c] Quan Shi *[a]

[a] Thermochemistry Laboratory, Liaoning Province Key Laboratory of Thermochemistry for Energy and Materials, Dalian National Laboratory for Clean Energy, Dalian Institute of Chemical Physics, Chinese Academy of Sciences, Dalian 116023, China.

[b] State Key Laboratory of Catalysis, Dalian Institute of Chemical Physics, Chinese Academy of Sciences, 457 Zhongshan Road, Dalian 116023, China.

[c] DICP-Surrey Joint Centre for Future Materials, Department of Chemical and Process Engineering and Advanced Technology Institute, University of Surrey, Guildford, Surrey, GU2 7XH, UK.

[d] University of Chinese Academy of Sciences, Beijing 100049, China

[e] Dalian Jiaotong University, School of Art and Design, Dalian 116028, China

*Corresponding Author: jian.liu@surrey.ac.uk

shiquan@dicp.ac.cn

Characterization

The morphology and structure were measured using a field-emission scanning electron microscopy (SEM，QUANTA 450) and transmission electron microscopy (TEM, JEM-2100, Japan). The pore properties and Brunauer–Emmett–Teller (BET) surface area were determined by nitrogen adsorption-desorption isotherm instrument (TriStar II 3020), and the pore-size distribution was calculated based on the DFT model. X-ray photoelectron spectroscopy (XPS，Escalab 250xi) was used to define the compositions and binding energy. Roman spectroscopy (Nano Wizard Ultra Speed & in Via Raman, German) was conducted to evaluate the graphitization degree of FCA with the excitation laser excitation of 532 nm. The chemical composition of PFC CPCMs was investigated using a fourier transform infrared (FTIR) spectrometer (Nicolet iS50) in the form of KBr discs over the range of 400-4000 cm^{-1} and X-ray diffractometer (XRD).

The phase change properties were investigated by means of a differential scanning calorimeter (Discovery DSC, TA, America) under nitrogen atmosphere. In the DSC measurements, the samples were heated from 40 °C to 100 °C and held at 100 °C for 3 min to erase the thermal history of the sample, following by cooling to -20 °C and then heated to 100 °C with a scanning rate of 10 ℃/min, and the second run was employed to analyze the phase change properties. The thermal stability was

determined using a thermogravimetric analyzer (TG, SETSYS 16/18, SETARAM, France) from room temperature to 600 °C with a heating rate of 10 °C/min under nitrogen atmosphere. The thermal conductivity measurement with an uncertainty of ± (2-5) % was performed on a thermal constants analyzer (Hot Disk TPS2500S) at room temperature. The thermal cycle stability was evaluated by 1000 heating-cooling cycles using a self-developed device. The magnetic property (M–H curve) was measured with a Quantum Design Physical Property Measurement System (PPMS-9, USA). The optical properties were studied using an ultraviolet–visible–near-infrared (UV–vis–NIR) spectrophotometer (Lambda 950, USA).

The solar-thermal conversion experiments were examined under a simulated sunlight provided by a xenon lamp source (Beijing Bofeilai Technology Co., Ltd, China), where the distance between sample and light source was set to be about 20 cm. The temperature was measured by a thermocouple and the data was collected by a data acquisition/ switch unit. The electro-thermal conversion property was tested by a direct current power supply. The temperature was measured by a thermocouple and the data was collected by a data acquisition unit. The magnetic-thermal conversion process was evaluated under an alternating magnetic field generated by an alternating current generator, and the temperature of the sample was detected using a fiber sensor. The infrared imaging photos

were taken by an infrared thermal imager (Fluke Ti400)

Table S1. Synthesis condition of different FCA and FCA CPCMs samples.

FCA samples	Gelatin (g)	$Fe(NO_3)_3 \cdot 9H_2O$ (g)	FCA CPCMs
FCA0	2	0	FCA0-C20
FCA1	2	1	FCA1-C20
FCA2	2	2	FCA2-C20
FCA3	2	3	FCA3-C20

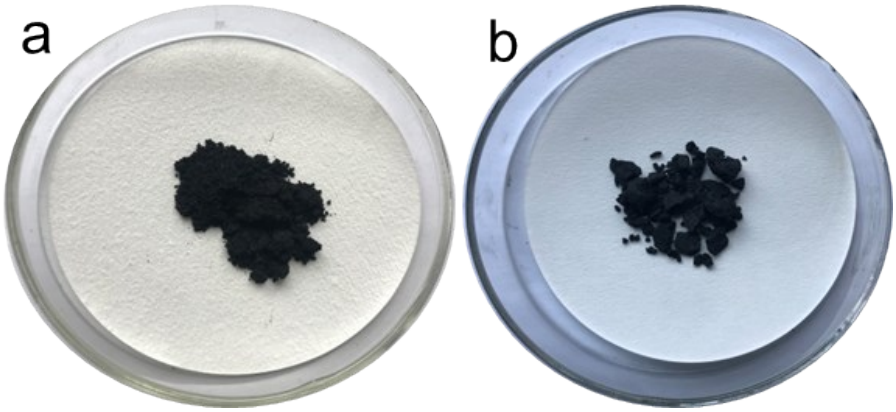

Figure S1. Photographs of (a) FCA and (b) FCA CPCMs.

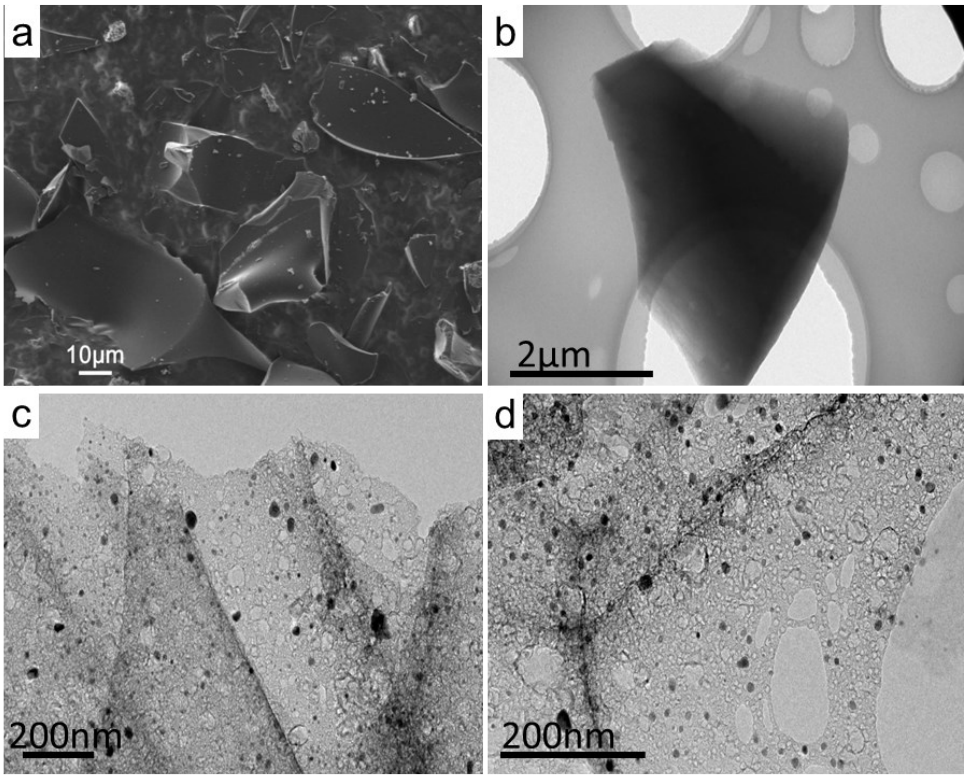

Figure S2. (a) SEM image of FCA0, (b) TEM images of FCA0 and (c, d) FCA2.

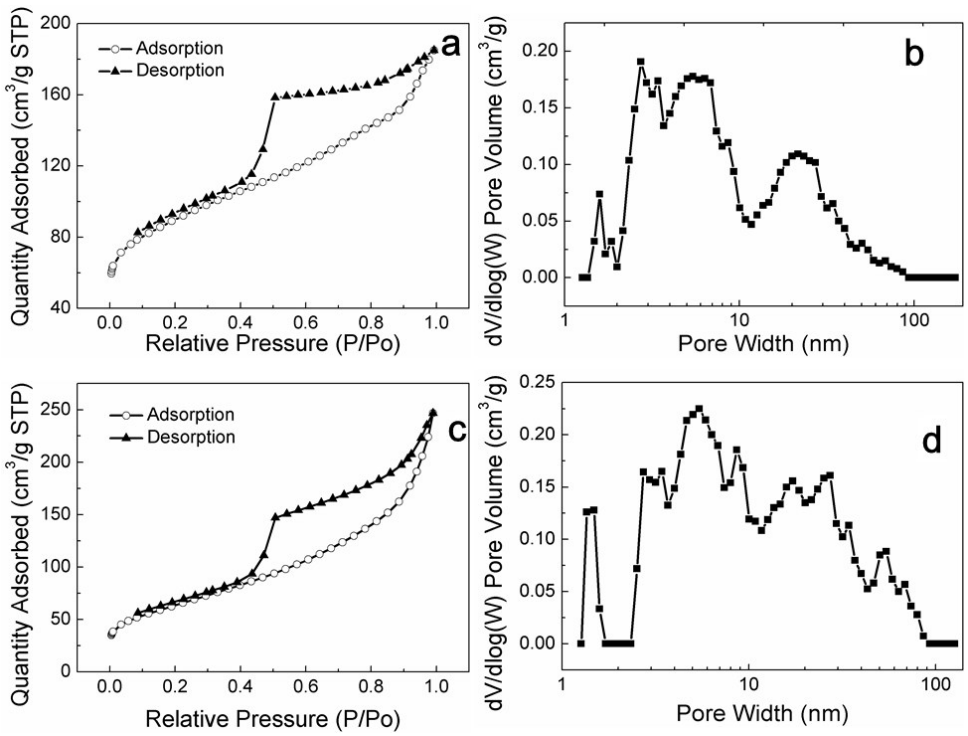

Figure S3. N_2 adsorption and desorption isotherms and corresponding pore size distributions of (a, b) FCA1 and (c, d) FCA3.

Table S2. N_2 adsorption and desorption data of FCA samples.

Sample	Surface area (m^2/g)	Average pore size (nm)
FCA1	301.63	4.31
FCA2	248.37	5.83
FCA3	228.35	6.61

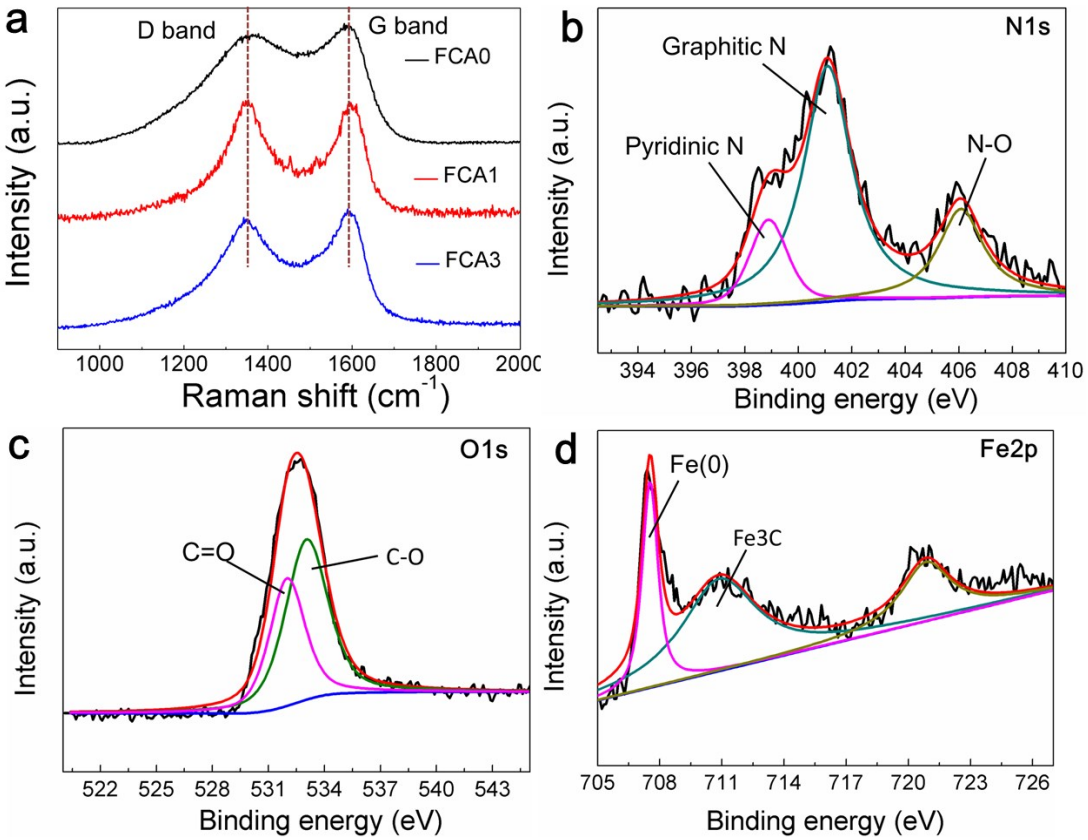

Figure S4. (a) Raman spectrums of FCA0, FCA1 and FCA3, (b) N1s, (C) O1s and (d) Fe2p spectra of FCA2.

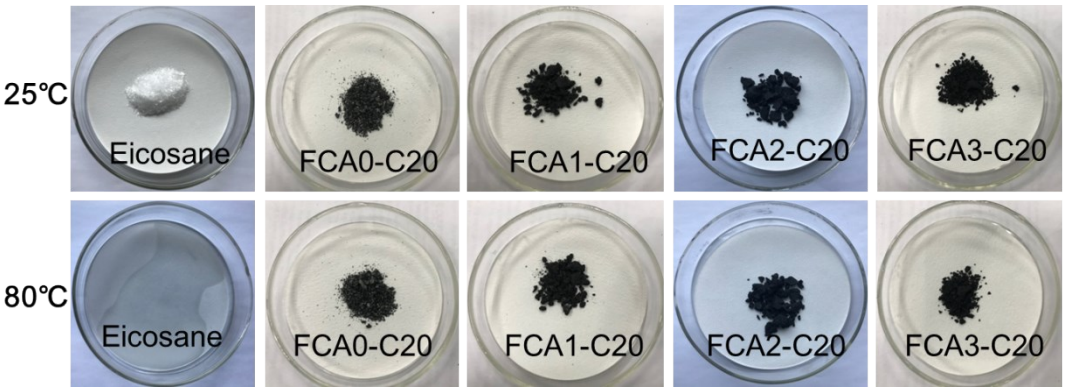

Figure S5. Leakage test photographs for eicosane, FCA0-C20, FCA1-C20, FCA2-C20 and FCA3-C20 sample.

Table S3. TG data of eicosane and FCA CPCMs samples.

Sample	T_{Onset} (°C)	Weight loss (%)	Eicosane ratio (%)
FCA0-C20	221.17	15.96	16.64
FCA1-C20	242.21	57.01	59.42
FCA2-C20	265.49	82.32	85.80
FCA3-C20	265.82	82.19	85.67
Eicosane	275.39	95.94	100

In the Table S3, T_{Onset} presents the decomposition temperature of sample. The eicosane ratio was determined by the following equation:

$$\text{Eicosane ratio (\%)} = \text{Weight loss(\%)}/95.94\%$$

Table S4. DSC data of eicosane and FCA CPCMs samples.

Sample	Melting progress		Crystallization process		R(%)	E(%)
	Onset(°C)	ΔH_m (J/g)	Onset(°C)	ΔH_c (J/g)		
FCA0-C20	35.32	52.86	34.34	52.34	20.98	20.99
FCA1-C20	35.18	150.05	34.42	148.99	59.57	59.66
FCA2-C20	35.03	211.66	34.36	209.80	84.03	84.09
FCA3-C20	35.27	210.93	34.09	208.63	83.74	83.71
Eicosane	35.80	251.89	33.93	249.31	100	100

To further determine the thermal energy storage property of FCA CPCMs samples, following equations were employed and the calculated results are list in Table S4:

$$R = \frac{\Delta Hm,CPCM}{\Delta Hm,PCM} \times 100\% \quad (1)$$

$$E = \frac{\Delta Hm,CPCM + \Delta Hc,CPCM}{\Delta Hm,PCM + \Delta Hc,PCM} \times 100\% \quad (2)$$

In the above equations, R and E represent the encapsulation ratio and encapsulation efficiency, and $\Delta H_{m,CPCM}$, $\Delta H_{c,CPCM}$, $\Delta H_{m,PCM}$ and $\Delta H_{c,PCM}$ are phase change enthalpy of FCA CPCMs and eicosane samples in melting and crystallization process, respectively.

Table S5. Thermal cycle stability data of FCA2-C20 sample.

Cycle times	Melting progress		Crystallization process	
	Onset(°C)	ΔH_m (J/g)	Onset(°C)	ΔH_c (J/g)
FCA2-C20	35.01	212.35	34.28	211.82
After 200 cycles	34.91	209.64	34.25	209.02
After 400 cycles	34.78	212.84	34.32	211.64
After 600 cycles	34.99	206.05	34.16	205.60
After 800 cycles	35.02	205.04	34.20	204.84
After 1000 cycles	35.00	205.23	34.13	204.67

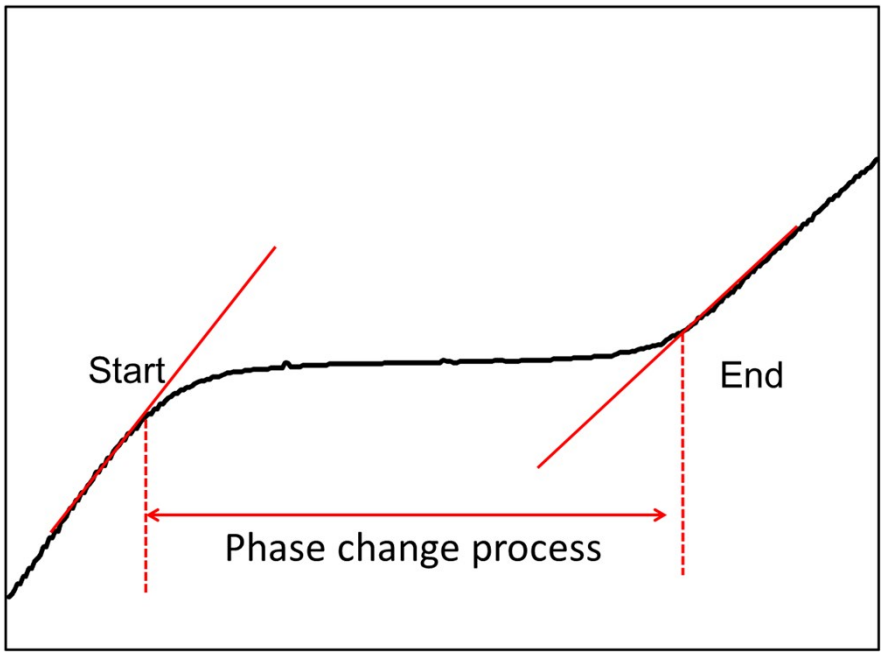

Figure S6. The schematic of tangential method.

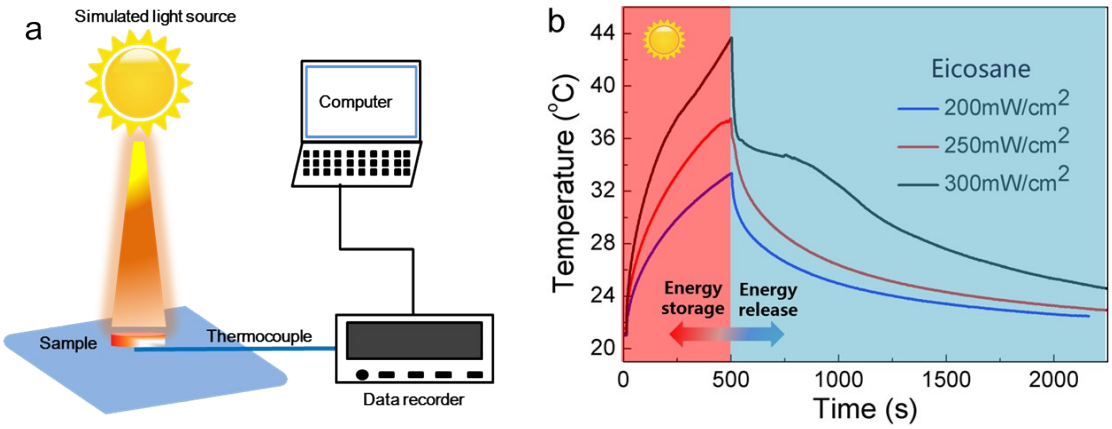

Figure S7. (a) The schematic of solar-thermal conversion device diagram, (b) solar-thermal conversion curves of eicosane.

Table S6. Solar-thermal conversion data of FCA2-C20 sample.

Sample	FCA2-C20		
Sample mass(g)	0.56		
Sample area (cm^2)	4.06		
Temperature (℃)	27-34		
C_p (J/(g.℃))	1.66(30.5℃)		
P (mW/cm^2)	200	250	300
Start time (s)	64	44	34
End time (s)	318	204	144
Δt (s)	254	160	110
Input energy [a] (J)	206.25	162.4	133.98
Thermal energy storage [b] (J)	125.04		
η (%)	60.63	77.00	93.32

[a]Input energy= $P * s * \Delta t$ [b]Thermal energy storage = $m * (\Delta H + Q)$

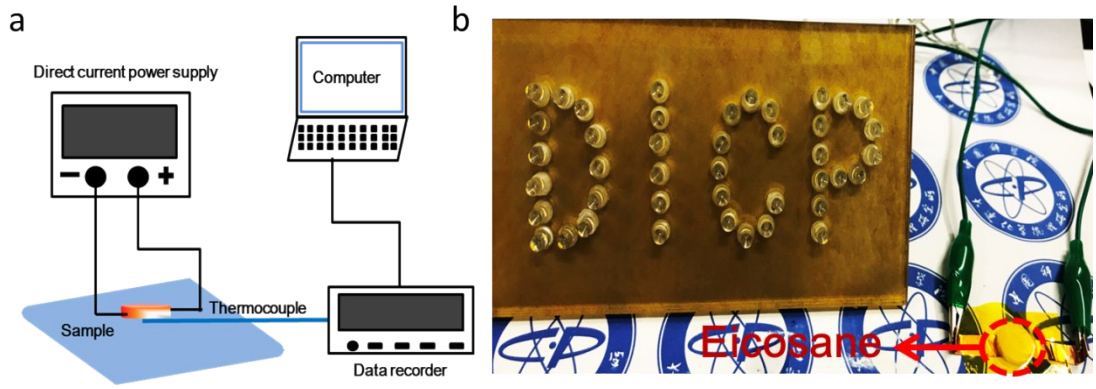

Figure S8. (a) The schematic of electro-thermal conversion device diagram. (b) LED lights of "DICP" symbols with eicosane sample.

Table S7. Electro-thermal conversion data of FCA2-C20 sample.

Sample	FCA2-C20		
Sample mass(g)	0.56		
Temperature (℃)	24-39		
C_p (J/(g.℃))	1.78(31.5℃)		
I (A)	0.12	0.15	0.20
Start time (s)	38	24	20
End time (s)	150	84	50
Δt (s)	112	60	30
Input energy [a] (J)	278.70	190.40	140.75
Thermal energy storage [b] (J)	133.48		
η (%)	47.89	70.11	94.83

[a]Input energy= $U * I * \Delta t$ [b]Thermal energy storage = $m * (\Delta H + Q)$

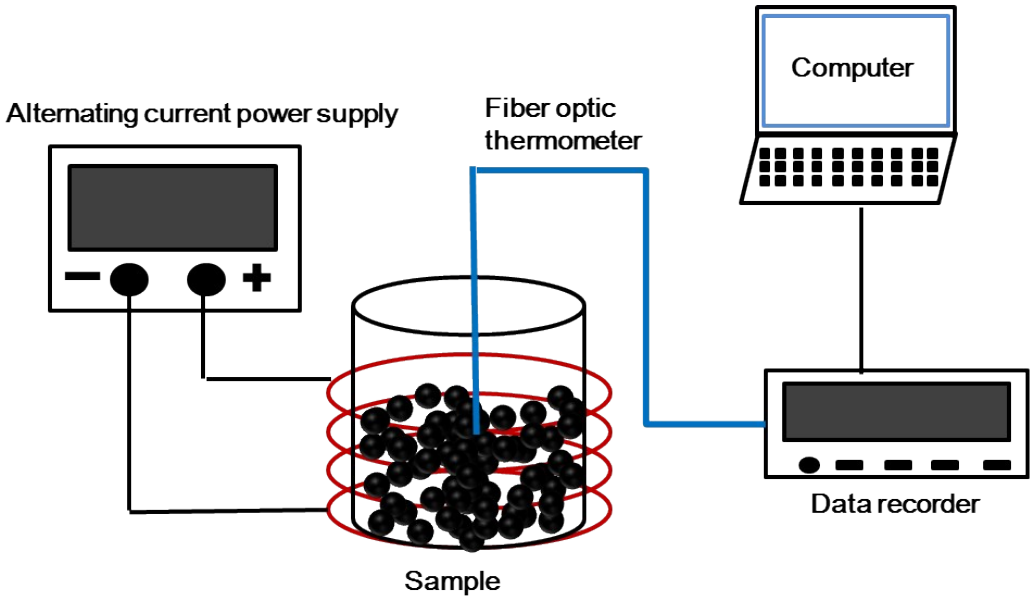

Figure S9. The schematic of magnetic-thermal conversion device diagram